Lithosphere

Azimuthal anisotropy in the Chile Ridge subduction region retrieved from ambient noise

A. Gallego, M.P. Panning, R.M. Russo, D. Comte, V.I. Mocanu, R.E. Murdie and J.C. Vandecar

Lithosphere 2011;3;393-400
doi: 10.1130/L139.1

Notes

Azimuthal anisotropy in the Chile Ridge subduction region retrieved from ambient noise

A. Gallego[1]*, M.P. Panning[1]*, R.M. Russo[1]*, D. Comte[2]*, V.I. Mocanu[3]*, R.E. Murdie[4]*, and J.C. Vandecar[5]*

[1]DEPARTMENT OF GEOLOGICAL SCIENCES, UNIVERSITY OF FLORIDA, P.O. BOX 112120, 241 WILLIAMSON HALL, GAINESVILLE, FLORIDA 32611, USA
[2]DEPARTMENT DE GEOFISICA, UNIVERSIDAD DE CHILE, BLANCO ENCALADA 2002, P.O. BOX 2777, SANTIAGO, CHILE
[3]DEPARTMENT OF GEOPHYSICS, BUCHAREST UNIVERSITY, 6 TRAIAN VUIA STREET, RO-7139 BUCHAREST 1, ROMANIA
[4]GOLD FIELDS AUSTRALIA, ST. IVES GOLD MINE, P.O. BOX 359, KAMBALDA, WA 6442, AUSTRALIA
[5]DTM, CARNEGIE INSTITUTE OF WASHINGTON, 2541 BROAD BRANCH ROAD, WASHINGTON, D.C. 20015, USA

ABSTRACT

In the southern Andes, the oblique convergence of the Nazca plate and the subduction of an active oceanic ridge represent two major tectonic features driving deformation of the forearc in the overriding continental plate, and the relative effects of these two mechanisms in the stress field have been a subject of debate. North of the Chile triple junction, oblique subduction of the Nazca plate is associated with the Liquiñe-Ofqui fault zone, an ~1000-km-long strike-slip fault that is partitioning the stress and deformation in the forearc. South of the Chile triple junction, the Antarctic plate converges normal to the trench, and several ridge segments have been colliding with the overriding plate since 14 Ma. Proposed effects of the collision include episodes of uplift, extension, and formation of a forearc sliver. Using ambient seismic noise recorded by the Chile Ridge Subduction Project seismic network, we retrieved azimuthal anisotropy from inversion of Rayleigh wave group velocity in the 6–12 s period range, mostly sensitive to crustal depths. North of the Chile triple junction in the forearc region, our results show a fast velocity for azimuthal anisotropy oriented subparallel to the Liquiñe-Ofqui fault zone. South of the Chile triple junction, anisotropy is higher, and fast velocity measurements present clockwise rotation south of the subducted ridge and counterclockwise rotation north of the ridge. These results suggest the presence of two main domains of deformation: one with structures formed during oblique convergence of the Nazca plate north of the Chile triple junction and the other with structures formed during normal convergence of the Antarctic plate, coupled with collision of the Chile Ridge south of the Chile triple junction. Low velocities and high anisotropy over the subducted Chile Ridge and slab window could be an indication of anomalously high thermal conditions, yielding a more plastic deformation compared with the north, where conditions are more cold and rigid.

LITHOSPHERE; v. 3; no. 6; p. 393–400; Data Repository Item 2011349. doi: 10.1130/L139.1

INTRODUCTION

In the Chile triple junction, subduction of the Nazca and Antarctic plates beneath South America controls the upper-plate state of stress and deformation (Figs. 1 and 2). Both oceanic plates are separated by an active oceanic spreading ridge and active transform faults (Cande and Leslie, 1986; Cande et al., 1987; Eagles et al., 2009; Breitsprecher and Thorkelson, 2009). South of the Chile triple junction, the Antarctic plate subducts normal to the trench at 1.85 cm/yr, and north of the Chile triple junction, the Nazca plate converges oblique to the trench at 6.6 cm/yr (Wang et al., 2008). Collision of ridge segments started at 14 Ma at Tierra del Fuego latitudes (55°S) and has been progressively migrating to the north to its current position at 46.5°S (Cande and Leslie, 1986). In the forearc, deformation induced by the oblique subduction of the Nazca plate and collision of the Chile ridge is accommodated by the Liquiñe-Ofqui fault zone, an active, dextral strike-slip fault with a length of ~1000 km that runs parallel to the active volcanic arc (Cembrano and Herve, 1993; Cembrano et al., 1996; Rosenau et al., 2006). The fault represents the eastern limit of a hypothesized forearc sliver that is currently moving northward (Forsythe and Nelson, 1985; Wang et al., 2008). Recent seismicity in the Aysen region clustered in the Liquiñe-Ofqui fault zone indicates a strike-slip fault mechanism along the fault (Mora et al., 2010; Russo et al., 2011).

Structural evidence of ridge interaction with the overriding plate includes episodes of crustal uplift (Ramos, 2005; Espinoza et al., 2005), opening of the Golfo de Penas Basin (Forsythe and Nelson, 1985), and block rotations of the Taitao ophiolite (Veloso et al., 2005). The combined effect of oblique subduction and ridge collision is invoked to explain transtensional deformation and a decrease in the stress gradient along the forearc toward the north (Nelson et al., 1993; Cembrano et al., 2002; Islam, 2009). In the subducted lithosphere, opening of the ridge results in the formation of a slab window, changing the thermal conditions of the mantle (Ramos and Kay, 1992; Murdie et al., 1993; Breitsprecher and Thorkelson, 2009; Russo et al., 2010a, 2010b) and overriding crust (Cande et al., 1987; Murdie at al., 1993) and affecting the elastic conditions and deformation style of the crust (Cembrano et al., 2002; Groome and Thorkelson, 2009). Previous studies of the seismic anisotropy in the upper mantle of the Chile triple junction area were based on shear-wave splitting of SKS and S phases. These results reveal that fast axes are parallel to the subducted spreading ridge segments of the Chile Rise, probably as a result of along-axis asthenospheric flow (Murdie and Russo, 1999). Subsequently, Russo et al. (2010a, 2010b) showed that anisotropy in this area is highly variable, with fast shear-wave propagation typically parallel to the trench north of the Chile triple junction, but more nearly normal to the trench near and south of the Taitao Peninsula.

*E-mails: agallego75@gmail.com; mpanning@ufl.edu; rrusso@ufl.edu; dcomte@dgf.uchile.cl; victor.mocanu@g.unibuc.ro; ruth.murdie@goldfields.com.au; jvandecar@hotmail.com.

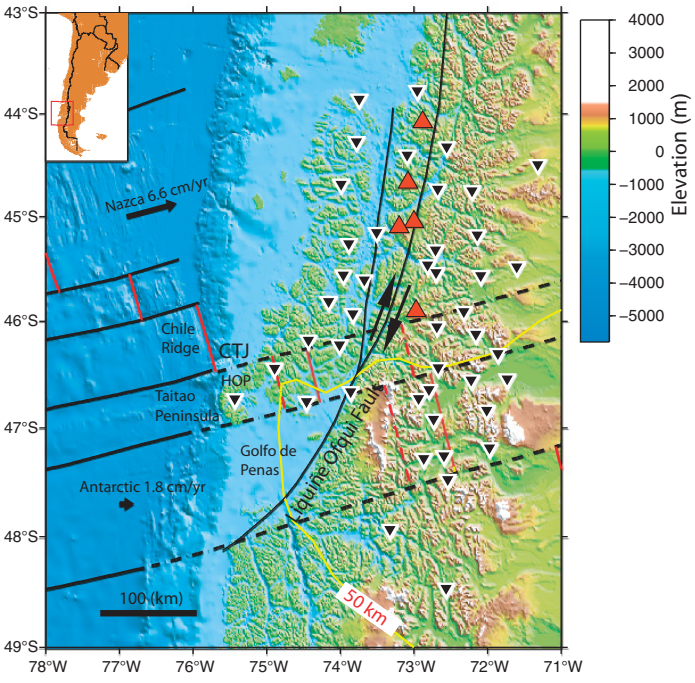

Figure 1. Tectonics and topography of Chile triple junction (CTJ) area. Black inverted triangles—seismic stations; red triangles—volcanoes (approximated limit of forearc and backarc regions); black and red lines—transform faults, fracture zones, and active ridge segments; dashed lines—surface projections (Murdie and Russo 1999). Arrows are relative convergence directions of Nazca (6.6 cm/yr) and Antarctic (1.8 cm/yr) plates (Wang et al., 2008). Double-stranded fault cutting the region is the Liquiñe-Ofqui fault zone. Yellow curved line—Patagonian slab window boundary defined by P wave tomography shown at 50 km depth (Russo et al., 2010).

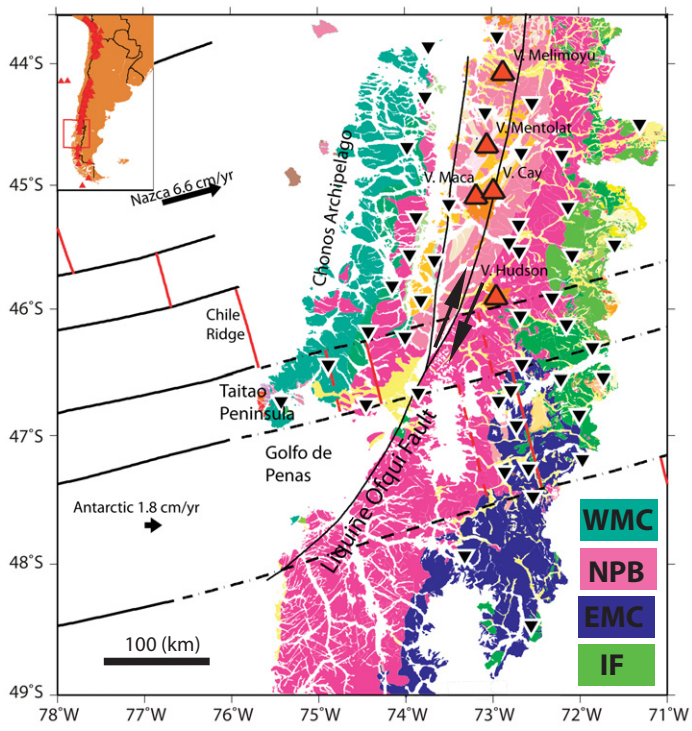

Figure 2. Geologic map of Chile triple junction region (from Gallego et al., 2010, after Escobar, 1980). Black inverted triangles represent seismic stations. Red triangles represent volcanoes (V.). WMC—Western metamorphic complex, NPB—North Patagonian Batholith, EMC—Eastern metamorphic complex, IF—Ibanez Formation. Description of units is given in supplementary material (see text footnote 1).

The geology of the study region (Fig. 2) is composed mainly of highly heterogeneous rocks of the Cenozoic–Mesozoic Northern Patagonian Batholith, which show mylonitization along the Liquiñe-Ofqui fault zone (Cembrano et al., 1996). The western boundary of the Northern Patagonian Batholith is formed by the foliated rocks of the Western metamorphic complex, and the eastern boundary is formed by Jurassic volcaniclastic rocks of the Ibanez Formation in the north and the Eastern metamorphic complex in the south (Escobar, 1980; Herve et al., 2008).

At different length scales, measurements of seismic anisotropy have been broadly used to constrain the mineralogy and dynamics of the crust and mantle (Silver, 1996; Maggi et al., 2006). The most likely cause of anisotropy in the mantle is the systematic crystal lattice-preferred orientation of anisotropic crystals during mantle flow (Hess, 1964; Mainprice and Silver, 1993). In the crust, variations of anisotropy may result from lattice-preferred orientation of minerals, parallel fractures or dikes, and metamorphic foliations (Crampin, 1994; Babuska and Cara, 1991). Several studies have used dispersion of short-period waves (1–20 s) originating from earthquakes to infer the phase velocity and azimuthal anisotropy in the upper crust (Levshin et al., 1992; Li and Detrick, 2003; Su et al., 2008), but few studies (Yao and van der Hilst, 2009; Fry et al., 2010) have used surface waves generated by ambient seismic noise to resolve anisotropy. One of the main problems with this technique is the possible bias effect between ray-path orientation and source noise distribution. Yet, Yao and van der Hilst (2009) demonstrated that incoherent noise has little effect (<1%) on the resulting isotropic phase velocities or azimuthal anisotropy.

In this study, we extend our results of isotropic velocities obtained for the Chile triple junction area using ambient noise of Rayleigh waves (Gallego et al., 2010), and we invert for azimuthal anisotropy in order to calculate the fast velocity directions of these waves. The results are used as a proxy to retrieve the current state of stress and deformation in the crust and their implications for the tectonic evolution of this area. Specifically, we address the effect of oblique subduction of the Nazca plate and normal subduction of the Antarctic plate, coupled with ridge collision, on the state of stress and deformation in crust of the Chile triple junction region.

METHODOLOGY

For this study, we used ambient seismic noise data obtained from 44 broadband sensors (Fig. 1) deployed between December 2004 and February 2007 in the Chile triple junction region. Dispersion data for Rayleigh wave group velocity were calculated in two steps. In the first step, for each station pair, we cross-correlated 24 h of data independently and then stacked them day by day into one time series that represents the Green's function dominated by Rayleigh wave energy for the given station pair (Bensen et al., 2007). In the second step, we used filter processing (Levshin et al., 1992) to calculate Rayleigh group velocity dispersion curves (Fig. 3). Details of data processing and data selection can be found in Gallego et al. (2010).

Seismic-wave velocities in an anisotropic medium depend on the direction of propagation. The wave velocity is not independent of the medium's elastic parameters, so the inversion for velocity also yields the value of these parameters and the trade-off between them. The azimuthal dependence of Rayleigh wave velocity in a slightly anisotropic medium has a

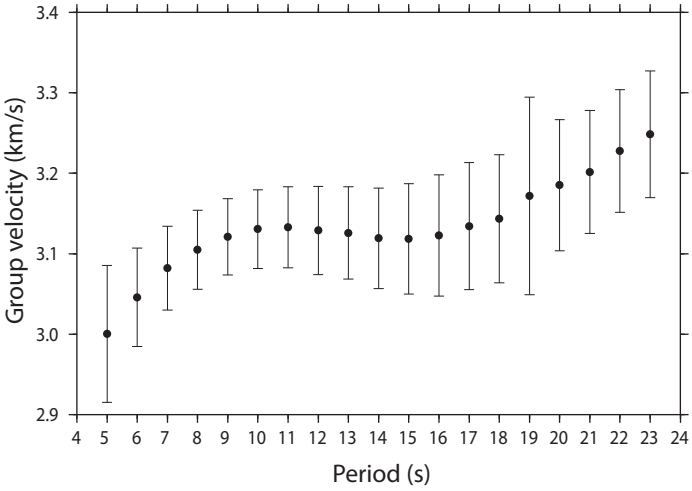

Figure 3. Path-averaged dispersion curves for Rayleigh wave group velocity. Error bars indicate standard deviation.

symmetry with 2θ and 4θ dependence, but 2θ terms are expected to dominate (Smith and Dahlen, 1973), and so can be written as

$$C(\omega,\theta) = C_0(\omega) + A_1\cos(2\theta) + A_2\sin(2\theta), \quad (1)$$

where C is the phase or group velocity, ω is the frequency of the wave, and θ corresponds to the azimuth along the path. The coefficient C_0 is the isotropic term, and A_i are the anisotropic coefficients for both Love and Rayleigh waves, which depend on the combinations of the elastic moduli through depth integration. The amplitude of the 2θ azimuthal anisotropy is defined as

$$\psi(2\theta) = \sqrt{A_1^2 + A_2^2}, \quad (2)$$

and the direction of the fast wave is defined to be:

$$\phi = \frac{1}{2}\tan^{-1}\frac{A_2}{A_1}. \quad (3)$$

Using the least-squared inversion developed by Tarantola (1982), the group velocity of Rayleigh waves was inverted simultaneously for the spatial distribution of the isotropic C_0 and anisotropic A_i terms. These terms were included in the matrix inversion,

$$m = m_{prior} + C_{i,a}G^t\left(GC_{i,a}G^t + C_D\right)^{-1}\left(d_{obs} - Gm_{prior}\right), \quad (4)$$

where G contains the lengths of segments formed by the intersections of ray paths and the cell boundaries, m is the matrix of slownesses of each cell block, and d is the interstation traveltime, obtained from the cross-correlation of stations pairs. G^t is the transposed value of G, m_{prior} is the a priori velocity model, which is assumed constant with average interstation velocities, C_D is a diagonal matrix of traveltime errors (assumed to be 2 s), and $C_{i,a}$ is the covariance matrix, derived from the exponential covariance function.

The inversion is mainly controlled by three parameters, the damping, L, the a priori standard deviation of isotropic terms, s_i, and the standard deviation for anisotropic terms, s_a, through the exponential covariance function:

$$C_{i,a}(x,x') = \sigma_{i,a}^2 \exp\left(\frac{-\|x-x'\|^2}{L}\right). \quad (5)$$

The optimal values for these parameters were selected by applying two synthetic checkerboard tests and a chi-squared statistical analysis. The first checkerboard tests (Figs. 4A and 4B) were constructed with alternating anisotropic blocks of 120 km by 120 km with velocity anomaly cells of 2 km/s and a fast velocity direction oriented E-W, and velocity anomaly cells of 3 km/s with a fast velocity oriented N-S. The inversion was performed using 665 ray paths, which is the number of ray paths obtained from the dispersion analysis for the 6 s period. The second checkerboard test (Figs. 4C and 4D) was constructed using a homogeneous layer with group velocity of 2 km/s and fast velocity oriented E-W and a N-S narrow anisotropic anomaly of 3 km/s with fast velocity oriented N-S, simulating the shear zone of the Liquiñe-Ofqui fault zone with the fast velocity parallel to the fault.

For the joint inversion, a good balance between over- and underfitting data was obtained using a damping parameter of L = 63.2 km, and standard deviations of σ_i (isotropic term) and σ_a (anisotropic term) equal to 0.07 km/s. The checkerboard test inversion was well resolved for isotropic and anisotropic terms. The elongated anomaly representing the Liquiñe-Ofqui fault zone was also well resolved, for both isotropic and anisotropic terms, especially between 44°S and 46°S, but at the edge of the ray-path coverage, the recovery of the resulting model presents some deviation from the synthetic model.

Ray-path distribution and resolution maps (Figs. 4A and 4B; see also GSA Data Repository[1]) of the anisotropic-joint inversion were included in the analysis. Resolution depends on ray-path density, the period of the Rayleigh waves, and the smoothing length used in the inversion

Our preferred anisotropic inversions were calculated with the C_0, A_1, and A_2 terms, and for test purposes, we included inversions for an isotropic-only model, determined without the A_i terms; an anisotropic-only model without the C_0 term; and resolution maps (supplementary material [see footnote 1]). In order to estimate the depth sensitivity of our models, we calculated partial derivatives inverting (Herrmann and Ammon, 2002) the averaged Rayleigh wave dispersion curves for variation of shear-wave velocity (Vs) with depth using a Preliminary Reference Earth Model (PREM) (Dziewonski and Anderson, 1981) starting model.

RESULTS

Inversion of Rayleigh wave group velocities resulted in four two-dimensional (2-D) models of azimuthal anisotropy with 2ψ symmetry at 6, 8, 10, and 12 s periods (Fig. 5). We obtained a maximum of 665 ray paths for Rayleigh waves at 6 s and a minimum of 340 ray paths at 12 s, with the best-resolved areas in two elongated zones covering the forearc and backarc regions (Fig. 6; supplementary material [see footnote 1]). Inversions for periods greater than 12 s resulted in poor ray coverage and were not included. Partial derivatives of Rayleigh wave group velocity with respect to S-wave velocity indicate sensitivities to crustal depths up to 20 km (Fig. 7). Most of the velocity anomalies obtained from the isotropic-only and anisotropic-only inversion can also be seen in the anisotropic joint model, indicating that the inclusion of the anisotropic terms does not introduce major artifacts into our final model (Data Repository [see footnote 1]). In general, isotropic velocities are higher in the forearc (>3.3 km/s), where the Western metamorphic complex is present, compared with the backarc (<3.2 km/s), which is formed mainly by rocks of the Northern Patagonian Batholith .

[1]GSA Data Repository Item 2011349, Inversion results for isotropic, pure anisotropic and joint inversion of Rayleigh wave group velocity, is available at www.geosociety.org/pubs/ft2011.htm, or on request from editing@geosociety.org, Documents Secretary, GSA, P.O. Box 9140, Boulder, CO 80301-9140, USA.

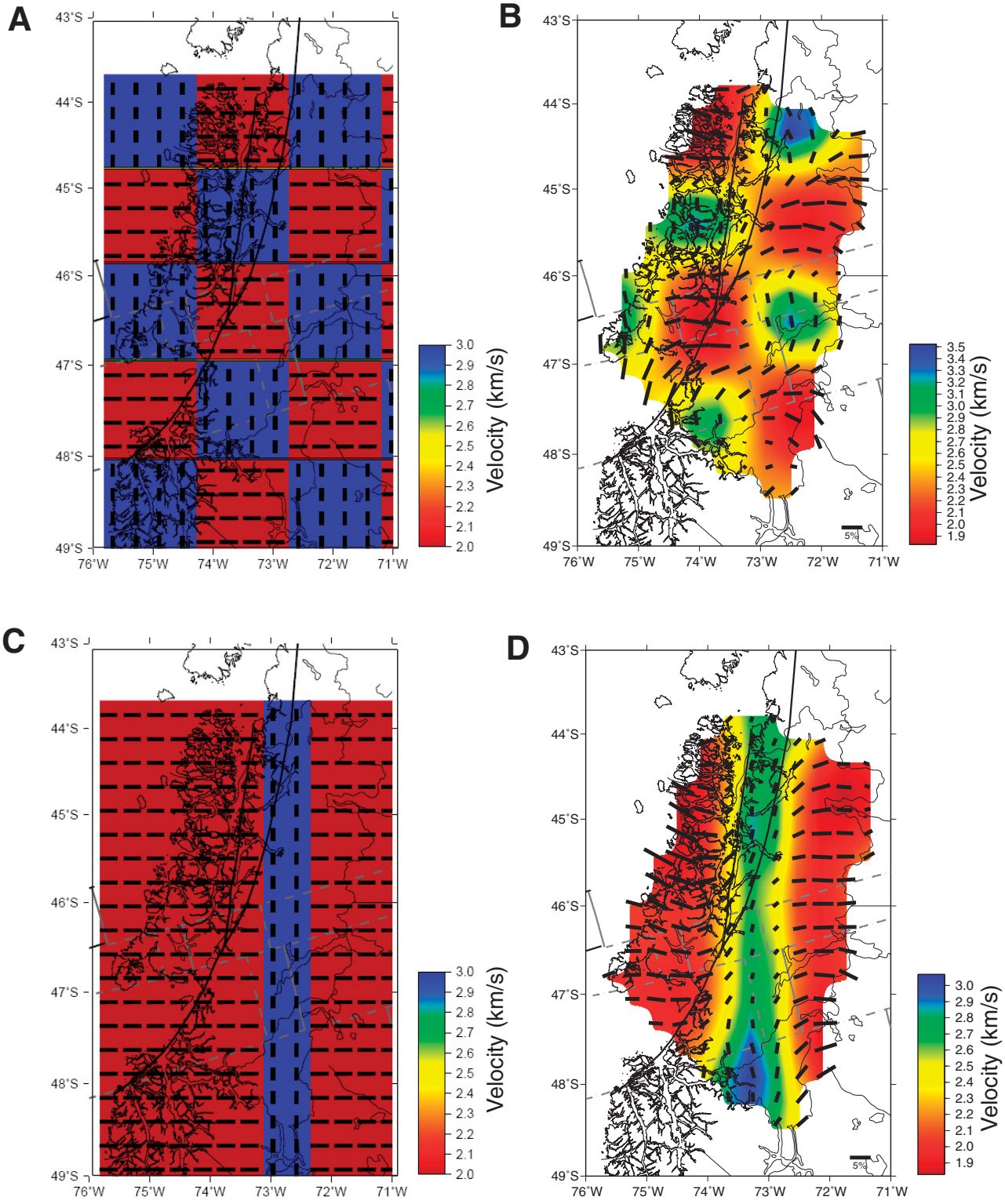

Figure 4. Checkerboard test of the study area. (A) Input anomalies with isotropic velocity blocks of 2 km/s and 3 km/s. (B) Isotropic and anisotropic joint inversion using 665 ray paths from synthetic model A. (C) Input anomalies include homogeneous bands of 2 km/s with E-W anisotropy and an elongated narrow band with a velocity of 3 km/s and N-S anisotropy. (D) Isotropic and anisotropic joint inversion using 665 ray paths from synthetic model C. Color bar indicates isotropic velocities, and black tick marks are strength and orientation of fast velocity.

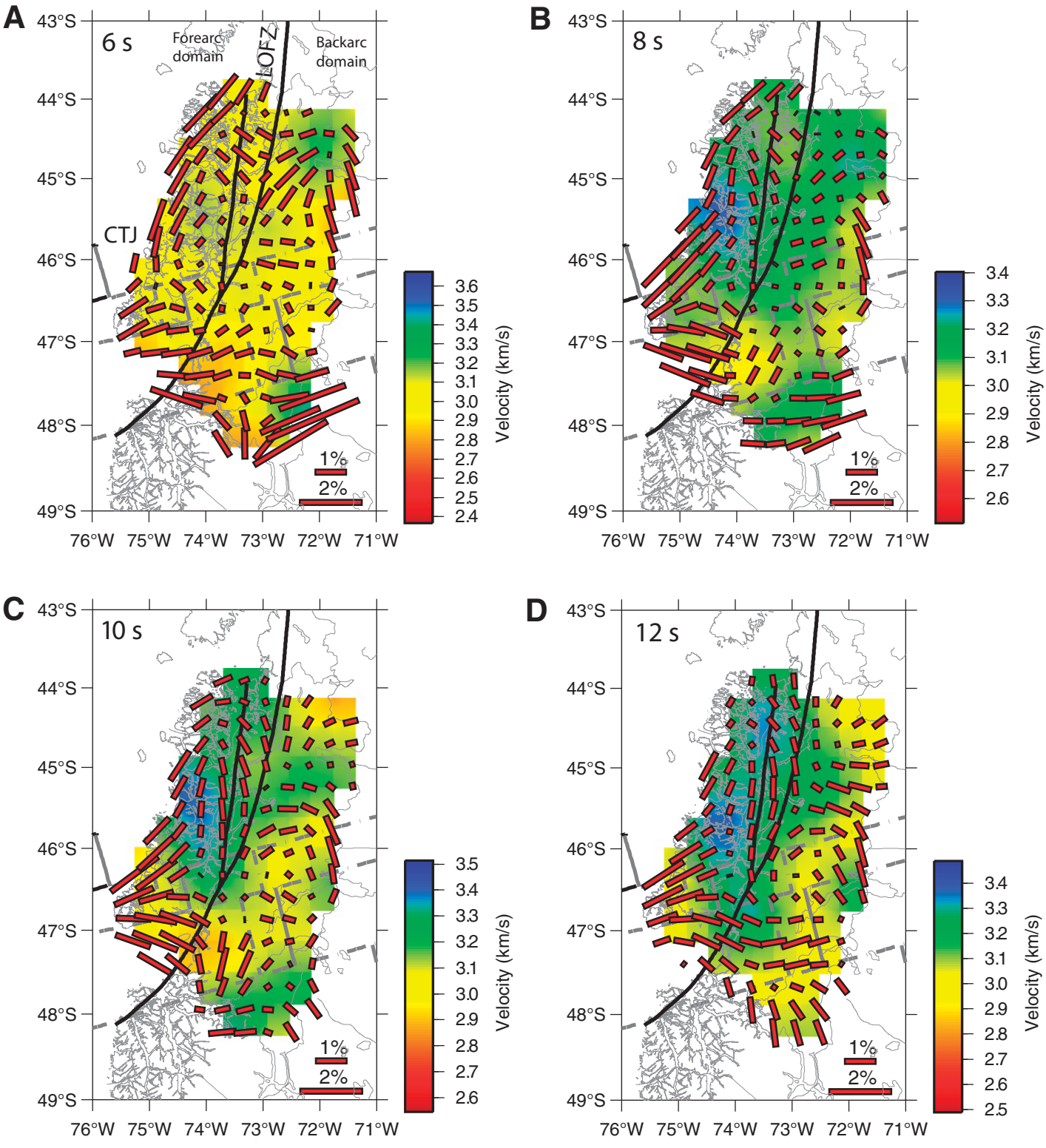

Figure 5. Isotropic and anisotropic joint inversion results for 6, 8, 10, 12 s periods of Rayleigh waves group velocity. Color bar indicates isotropic velocities, and red tick marks are strength and orientation of fast velocity. LOFZ—Liquiñe-Ofqui fault zone; CTJ—Chile triple junction.

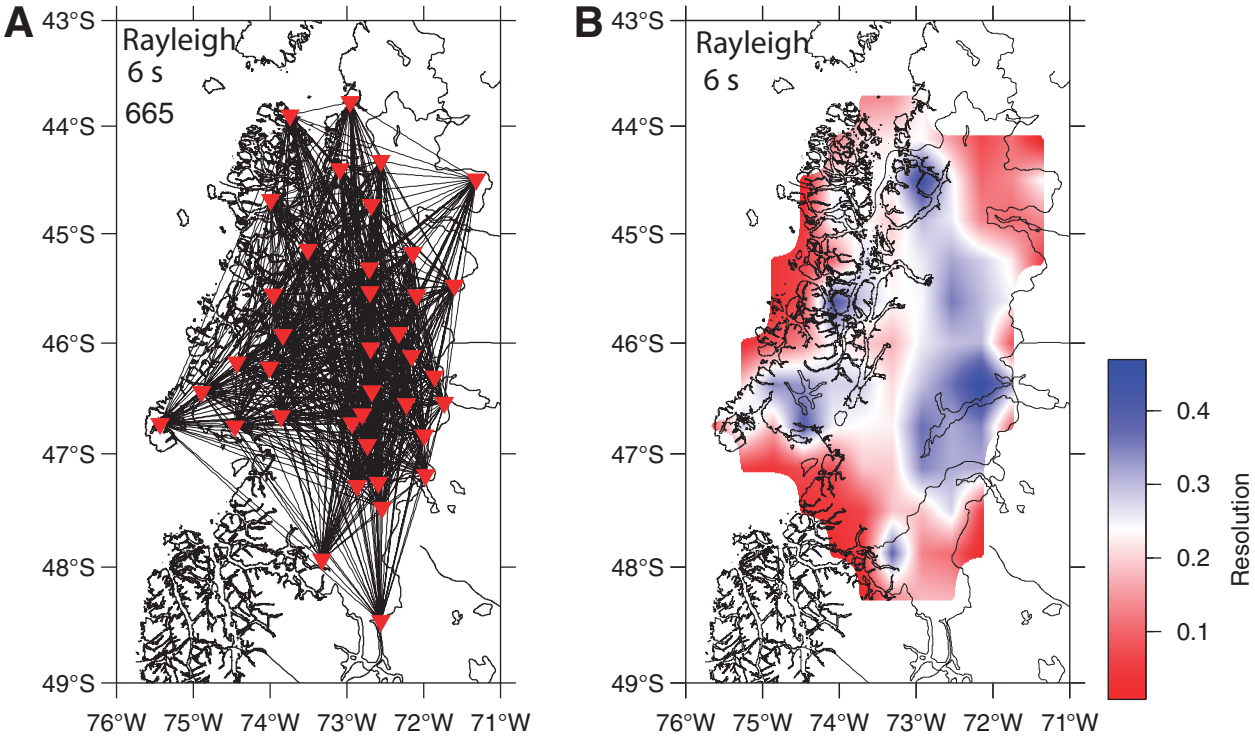

Figure 6. (A) Interstation ray-path coverage for 6 s period of Rayleigh waves. (B) Resolution calculation for 6 s period of Rayleigh waves.

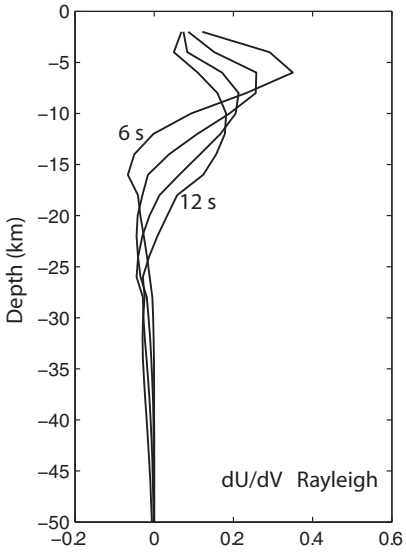

Figure 7. Rayleigh wave group velocity partial derivatives with respect to S-wave velocity for 6–12 s period.

South of the Chile triple junction, where the Chile ridge is subducting beneath South America, resolved maps in the 6–12 s period range reveal low isotropic velocities (<3.1 km/s), high azimuthal anisotropy (>1.6%), and a fast velocity with clockwise rotation south of the subducted ridge and counterclockwise rotation north of the subducted ridge in a fan-shaped pattern. To the north of the forearc, isotropic velocities increase (>3.2 km/s), azimuthal anisotropy decreases, and the fast velocity is oriented subparallel to the Liquiñe-Ofqui fault zone, with variations to the NNE and NNW. Resolution in the western edge of the forearc and Golfo de Penas is partial. However, when the inversion was run without station HOP (Fig. 1), located on the western edge of the Taitao Peninsula, we obtained similar azimuthal anisotropy patterns immediately east of the low-resolution area.

Compared with the forearc, the azimuthal anisotropy in the backarc region appears variable in strength and orientation, with no consistent anisotropy at the different periods. However, in the southeast over the Eastern metamorphic complex, at 6–8 s periods, high anisotropy (>2%) and high velocity (>3.1 km/s) are noticeable, with fast direction oriented E-W, yet inversion is not well resolved in this area.

DISCUSSION AND CONCLUSIONS

Azimuthal anisotropy (Fig. 5) obtained from inversion of ambient noise suggests that crustal deformation in the forearc is controlled by the subduction of the Chile Ridge and the dextral motion of the Liquiñe-Ofqui fault zone.

The main source of anisotropy in the crust is associated with the orientation of vertical filled cracks in shear zones (Crampin et al., 1994) and mineral alignment produced by shear deformation in a ductile regime (Babuska and Cara, 1991). Difficult to detect anisotropy in the crust arises due to lithological and structural inhomogeneities; however, laboratory tests show that anisotropy in mylonites formed during tectonism increases with the degree of deformation (Kern and Wenk, 1990; Shaocheng and Salisbuty, 1993).

In the forearc region, south of the Chile triple junction, where the Antarctic plate converges normal to the trench, and the Chile Ridge is subducting with strike N15°W, inversion in the 6–12 s range reveals con-

sistent low isotropic velocities (<3.1 km/s) and high azimuthal anisotropy (1.5%–2%). The fast axis direction shows clockwise rotation south of the Chile Ridge and counterclockwise rotation north of the ridge in a fan-shaped pattern. Toward the north, isotropic velocities are higher (>3.1 km/s), and the azimuthal anisotropy (0.5%–1%) decreases, with fast velocity subparallel to the strike of the Liquiñe-Ofqui fault zone. The observed anisotropy in the forearc south of the Chile triple junction may result from crack alignment during collision of the Chile Ridge with the South America plate. North of the Chile triple junction, fast velocity may be related to the Liquiñe-Ofqui shear zone and the oblique convergence of the Nazca plate. Similar deformation in the forearc has been observed in finite-element models that incorporate the effects of oblique subduction of the Nazca plate in the north and normal subduction of the Antarctic plate in the south (Nelson et al., 1994; Islam, 2009). For instance, calculations of Nelson et al. (1994) show a maximum horizontal stress and potential right-lateral faults that show clockwise rotation south of the Chile triple junction, counterclockwise rotation north of the Chile triple junction, and fast velocity subparallel to the north along the Liquiñe-Ofqui fault zone. This resembles the patterns of azimuthal anisotropy found in this study (Fig. 8), suggesting that the directions of fast velocities observed represent two areas with different styles of deformation: one with oblique convergence with respect to the trench and the other with normal convergence and ridge collision. Structural data of dike swarms distributed between 43°S and 48°S also show a preferred orientation NNE and N-S, coincident with the Liquiñe-Ofqui fault zone structures (Lefort et al., 2006). The low isotropic velocity and high anisotropy we observed south of the Chile triple junction could be an indication of higher temperatures due to the presence of the ridge subduction and slab window, enhancing the deformation as suggested by Cembrano et al. (2002) and Groome and Thorkelson (2009).

We also see correlation between anisotropy in the mantle from SKS shear-wave splitting and azimuthal anisotropy in this study. Splitting fast directions in the forearc are typically parallel to the trench north of the Chile triple junction, but they are more nearly normal to the trench near and south of the Chile triple junction (Russo et al., 2010). This suggests some level of coupling between the lithospheric mantle and the upper crust; however, our short period range does not permit a more conclusive explanation for this correlation.

In the backarc region, the variable azimuthal anisotropy observed could be related to rheological heterogeneities formed during magma emplacement, or it could indicate the presence of more stable upper crust at the east end of the Liquiñe-Ofqui fault zone, which is accommodating most of the deformation. The high anisotropy observed at 6–8 s in the southeast part of the map could be related to the deformed rocks of the Eastern metamorphic complex, but resolution in this area is poor.

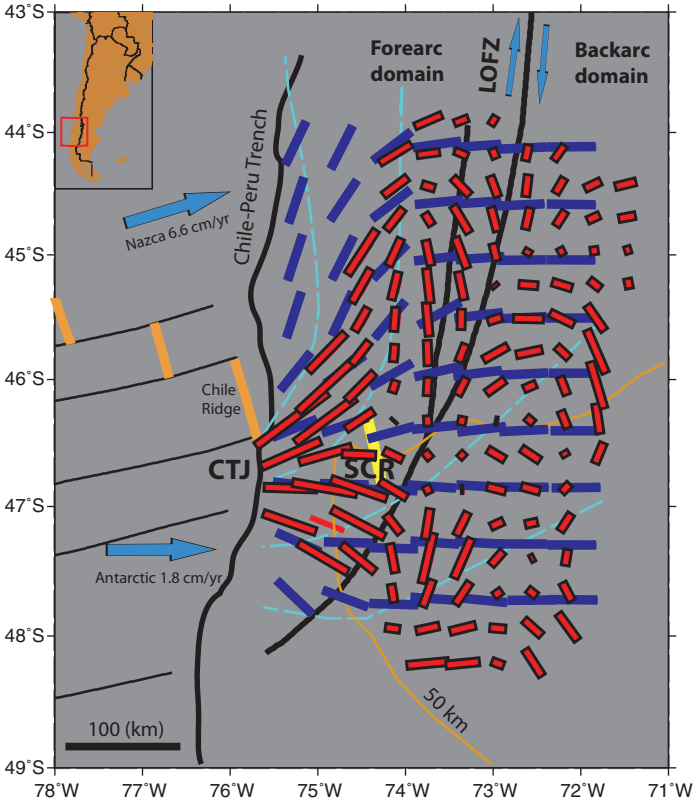

Figure 8. Comparison of maximum horizontal shear stress (light-blue dashed line) and potential right-lateral faults (blue tick marks) calculated with finite-element modeling from Nelson et al. (1993), with the predicted azimuthal anisotropy fast velocity (red tick marks) using inversion of Rayleigh waves at 10 s period in this study. Orange straight lines represent the Chile Ridge segments, yellow straight line is the projection of the subducted Chile Ridge (SCR), and the orange curve is the Patagonian slab window boundary as defined by P-wave tomography shown at 50 km depth (Russo et al., 2010). LOFZ—Liquiñe-Ofqui fault zone; CTJ—Chile triple junction.

ACKNOWLEDGMENTS

This work would not have been possible without the help of the following people: Umberto Fuenzalida, Hernan Marilao, and Carmen Gloria of the Universidad de Chile; Juan Fica, Claudio Manzur, Carlos Llautureo, Corporacion Nacional Forestal de Chile (CONAF); Monica Retamal Maturana, Banco Estado; Carabineros de Chile del Region de Aysen; Armada de Chile; Cuerpo Militar de Trabajo del Ejercito de Chile, Cmdte. Roldan, Maj. Wellkner; Luis Miranda Chiguay, Alcaldes de Aysen, Melinka, Rio Ibanez, Lago Verde; Ejercito de Chile; Carlos Feliu Ruiz, Aeronautica de Chile; Don Luis Hidalgo, Automotriz Varona; Don Gustavo Lopez y Hostal Bon; Mike Fort, Noel Barstow, Bruce Beaudoin, Jim Fowler of IRIS PASSCAL; Juan Gallardo, Axel Hernandez, Hernan Aguilar, Jose Geicha Nauto, Tripulacion de LM Petrel IV (CONAF); Gilles Rigaud, Aurelia Rigaud, Valerie Clouard, Lorena Palacio et Morgane; Eduardo Moscoso; Don Raul Hernandez, Fundo Los Nirres; Sergio Mirando Contreras (Melinka); Victor Figueroa, Escuela Carlos Condell, Calete Andrade, Puerto Aguirre; Enrique Alcalde (Cochrane); Luis Levin (Bahia Murta); Baterias GAMI (Puerto Montt); Mauricio Zambrano L. (Coyhaique Centro de Llamadas); Rolando Burgos and Roselia Delgado, Fachinal; Aladin Jara, Gobernacion de Chile Chico; Rolando Toloza, Ministerio Obras Publicas; Mark and Sra. Knipreth, Heart of the Andes Lodge; Heraldo Zapata Rivera, Ramon Villegas, Omar Tapia Vidal, Jorge Oyarzun Inostroza, Tripulacion de El Aleph; Sandalio Munoz, Fundo La Pedregosa; Don Cristian Brautigam; and the many, many people of Region XI, Aysen, who helped us enthusiastically and unstintingly and without whom this work would have been impossible. We thank Eric Nelson for his data included in our Figure 8 and anonymous reviewers for their constructive comments. This work was supported by U.S. National Science Foundation grant EAR-0126244 and CONICYT-CHILE grant 1050367.

REFERENCES CITED

Babuska, V., and Cara, M., 1991, Seismic Anisotropy in the Earth: London, Kluwer Academic Publisher, 217 p.

Bensen, G.D., Ritzwoller, M.H., Barmin, M.P., Levshin, A.L., Lin, F., Moschetti, M.P., Shapiro, N.M., and Yang, Y., 2007, Processing seismic ambient noise data to obtain reliable

broad-band surface wave dispersion measurements: Geophysical Journal International, v. 169, p. 1239–1260, doi:10.1111/j.1365-246X.2007.03374.x.
Breitsprecher, K., and Thorkelson, D.J., 2009, Neogene kinematic history of Nazca-Antarctic-Phoenix slab windows beneath Patagonia and the Antarctic Peninsula: Tectonophysics, v. 464, p. 10–20, doi:10.1016/j.tecto.2008.02.013.
Cande, S.C., and Leslie, R.B., 1986, Late Cenozoic tectonics of the southern Chile trench: Journal of Geophysical Research, v. 91, p. 471–496, doi:10.1029/JB091iB01p00471.
Cande, S.C., Leslie, R.B., Parra, J.C., and Hobart, M., 1987, Interaction between the Chile Ridge and Chile Trench: Geophysical and geothermal evidence: Journal of Geophysical Research–Solid Earth and Planets, v. 92, p. 494–520.
Cembrano, J., and Herve, F., 1993, The Liquiñe-Ofqui fault zone: A major Cenozoic strike-slip duplex in the Southern Andes, *in* Proceedings, 2nd International Symposium on Andean Geodynamics: Oxford, p. 175–178.
Cembrano, J., Herve, F., and Lavenu, A., 1996, The Liquiñe Ofqui fault zone: A long-lived intra-arc fault system in southern Chile: Tectonophysics, v. 259, p. 55–66, doi:10.1016/0040-1951(95)00066-6.
Cembrano, J., Lavenu, A., Raynolds, P., Arancibia, G., Lopez, G., and Sanhueza, A., 2002, Late Cenozoic transpressional ductile deformation north of the Nazca–South America–Antarctica triple junction: Tectonophysics, v. 354, p. 289–314, doi:10.1016/S0040-1951(02)00388-8.
Crampin, S., Chesnokov, E.M., and Aipkin, R.G., 1994, Seismic anisotropy: The state of the art: Geophysical Journal of the Royal Astronomical Society, v. 76, p. 1–16.
Dziewonski, A.M., and Anderson, D.L., 1981, Preliminary reference Earth model: Physics of the Earth and Planetary Interiors, v. 25, p. 297–356, doi:10.1016/0031-9201(81)90046-7.
Eagles, G., Gohl, K., and Larter, R.D., 2009, Animated tectonic reconstruction of the Southern Pacific and alkaline volcanism at its convergent margins since Eocene times: Tectonophysics, v. 464, p. 21–29, doi:10.1016/j.tecto.2007.10.005.
Escobar, T., 1980, Mapa Geológico de Chile: Santiago, Chile, Servicio de Geologia y Mineria, scale 1:1,000,000.
Espinoza, F., Morata, D., Pelleter, E., Maury, R.C., Suarez, M., Lagabrielle, Y., Polve, M., Bellon, H., Cotten, J., De la Cruz, R., and Guivel, C., 2005, Petrogenesis of the Eocene and Mio-Pliocene alkaline basaltic magmatism in Meseta Chile Chico, southern Patagonia, Chile: Evidence for the participation of two slab windows: Lithos, v. 82, p. 315–343, doi:10.1016/j.lithos.2004.09.024.
Forsythe, R., and Nelson, E., 1985, Geological manifestations of ridge collision—Evidence from the Golfo de Penas Taitao Basin, southern Chile: Tectonics, v. 4, p. 477–495, doi:10.1029/TC004i005p00477.
Fry, B., Deschamps, F., Kissling, E., Stehly, L., and Giardini, D., 2010, Layered azimuthal anisotropy of Rayleigh wave phase velocities in the European Alpine lithosphere inferred from ambient noise: Earth and Planetary Science Letters, v. 297, p. 95–102, doi:10.1016/j.epsl.2010.06.008.
Gallego, A., Russo, R.M., Comte, D., Mocanu, V.I., Murdie, R.E., and Vandecar, J.C., 2010, Seismic noise tomography in the Chile Ridge subduction region: Geophysical Journal International, v. 182, p. 1478–1492, doi:10.1111/j.1365-246X.2010.04691.x.
Groome, W., and Thorkelson, D., 2009, The three-dimensional thermo-mechanical signature of ridge subduction and slab window migration: Tectonophysics, v. 464, p. 70–83, doi:10.1016/j.tecto.2008.07.003.
Herrmann, R.B., and Ammon, J.B., 2002, Computer Programs in Seismology: Surface Waves, Receiver Functions and Crustal Structure: St. Louis, Missouri, St. Louis University, http://www.eas.slu.edu/People/RBHerrmann/ComputerPrograms.html.
Herve, F., Calderon, M., and Faundez, V., 2008, The metamorphic complexes of the Patagonian and Fuegian Andes: Geologica Acta, v. 6, p. 43–53.
Hess, H., 1964, Seismic anisotropy of the uppermost mantle under oceans: Nature, v. 203, p. 629–631, doi:10.1038/203629a0.
Islam, R., 2009, Origin of the regional stress field along the Liquiñe Ofqui fault zone (LOFZ), southern Chilean Andes, by means of FE simulation: Journal of Mountain Science, v. 6, p. 1–13, doi:10.1007/s11629-009-0253-x.
Kern, H., and Wenk, H.R., 1990, Fabric-related velocity anisotropy and shear wave splitting in rocks from the Santa Rosa mylonite zone, California: Journal of Geophysical Research, v. 95, p. 11,213–11,223, doi:10.1029/JB095iB07p11213.
Lefort, J.P., Aifa, T., and Herve, F., 2006, Structural and AMS study of a Miocene dike swarm located above the Patagonian subduction, *in* Hanski, E., Mertanen, S., Rämö, T., and Vuollo, J., eds., Dyke Swarms—Time Markers of Crustal Evolution: London, Taylor & Francis Group, p. 225–241.
Levshin, A., Ratnikova, L., and Berger, J., 1992, Peculiarities of surface-wave propagation across central Eurasia: Bulletin of the Seismological Society of America, v. 82, p. 2464–2493.
Li, A.B., and Detrick, R.S., 2003, Azimuthal anisotropy and phase velocity beneath Iceland: Implication for plume-ridge interaction: Earth and Planetary Science Letters, v. 214, p. 153–165, doi:10.1016/S0012-821X(03)00382-0.
Maggi, A., Debayle, E., Priestley, K., and Barruol, G., 2006, Azimuthal anisotropy of the Pacific region: Earth and Planetary Science Letters, v. 250, p. 53–71, doi:10.1016/j.epsl.2006.07.010.
Mainprice, D., and Silver, P.G., 1993, Interpretation of SKS-waves using samples from the subcontinental lithosphere: Physics of the Earth and Planetary Interiors, v. 78, p. 257–280, doi:10.1016/0031-9201(93)90160-B.
Mora, C., Comte, D., Russo, R., Gallego, A., and Mocanu, V., 2010, Aysen seismic swarm (January 2007) in southern Chile: Analysis using joint hypocenter determination: Journal of Seismology, v. 14, no. 4, p. 683–691, doi:10.1007/s10950-010-9190-y.
Murdie, R.E., and Russo, R.M., 1999, Seismic anisotropy in the region of the Chile Margin Triple Junction: Journal of South American Earth Sciences, v. 12, p. 261–270, doi:10.1016/S0895-9811(99)00018-8.
Murdie, R., Prior, D.J., Styles, P., and Flint, S.S., 1993, Seismic responses to ridge-transform subduction: Chile triple junction: Geology, v. 21, p. 1095–1098, doi:10.1130/0091-7613(1993)021<1095:SRTRTS>2.3.CO;2.
Nelson, R., Forsythe, R., and Arit, I., 1994, Ridge collision tectonics in terrane development: Journal of South American Earth Sciences, v. 7, no. 3/4, p. 271–278.
Ramos, V.A., 2005, Seismic ridge subduction and topography: Foreland deformation in the Patagonian Andes: Tectonophysics, v. 399, p. 73–86, doi:10.1016/j.tecto.2004.12.016.
Ramos, V.A., and Kay, S.M., 1992, Southern Patagonian plateau basalts and deformation: Back-arc testimony of ridge collision: Tectonophysics, v. 205, p. 261–282, doi:10.1016/0040-1951(92)90430-E.
Rosenau, M., Melnick, D., and Echtler, H., 2006, Kinematic constraints on intra-arc shear and strain partitioning in the southern Andes between 38°S and 42°S latitude: Tectonics, v. 25, TC4013, doi:10.1029/2005TC001943.
Russo, R.M., Gallego, A., Comte, D., Mocanu, V.I., Murdie, R.E., and VanDecar, J.C., 2010a, Source-side shear wave splitting and upper mantle flow in the Chile Ridge subduction region: Geology, v. 38, p. 707–710, doi:10.1130/G30920.1.
Russo, R.M., VanDecar, J.C., Comte, D., Mocanu, V.I., Gallego, A., and Murdie, R.E., 2010b, Subduction of the Chile Ridge: Upper mantle structure and flow: GSA Today, v. 20, no. 9, p. 4–10, doi:10.1130/GSATG61A.1.
Russo, R.M., Gallego, A., Comte, D., Mocanu, V.I., Murdie, R.E., Mora, C., and VanDecar, J.C., 2011, Triggered seismic activity in the Liquiñe-Ofqui fault zone, southern Chile, during 2007 Aysen seismic swarm: Geophysical Journal International, v. 184, no. 3, p. 1317–1326, doi:10.1111/j.1365-246X.2010.04908.x.
Shaocheng, J., and Salisbury, M., 1993, Shear-wave velocities, anisotropy and splitting in high-grade mylonites: Tectonophysics, v. 221, p. 453–473.
Silver, P.G., 1996, Seismic anisotropy beneath the continents: Probing the depths of geology: Annual Review of Earth and Planetary Sciences, v. 24, p. 385–432, doi:10.1146/annurev.earth.24.1.385.
Smith, M.L., and Dahlen, F.A., 1973, Azimuthal dependence of Love and Rayleigh-wave propagation in a slightly anisotropic medium: Journal of Geophysical Research, v. 78, p. 3321–3333, doi:10.1029/JB078i017p03321.
Su, W., Wang, C.Y., and Huang, Z.X., 2008, Azimuthal anisotropy of Rayleigh waves beneath the Tibetan Plateau and adjacent areas: Science in China, ser. D, Earth Science, v. 51, p. 1717–1725.
Tarantola, A., 1982, Generalized nonlinear inverse problems solved using least squares criterion: Reviews of Geophysics and Space Physics, v. 20, p. 219–232, doi:10.1029/RG020i002p00219.
Veloso, E., Anma, R., and Yamazaki, T., 2005, Tectonic rotations during the Chile Ridge collision and obduction of the Taitao ophiolite (southern Chile): The Island Arc, v. 15, p. 599–615.
Wang, K., Hu, Y., Bevis, M., Kendrick, E., Smalley, R., Vargas, R.B., and Lauria, E., 2008, Crustal motion in the zone of the 1960 Chile earthquake: Detangling earthquake-cycle deformation and forearc-sliver translation: Geochemistry Geophysics Geosystems, v. 9, Q10010, doi:10.1029/2007GC001869.
Yao, H.J., and van der Hilst, R.D., 2009, Analysis of ambient noise energy distribution and phase velocity bias in ambient noise tomography, with application to SETibet: Geophysical Journal International, v. 179, p. 1113–1132, doi:10.1111/j.1365-246X.2009.04329.x.

MANUSCRIPT RECEIVED 12 FEBRUARY 2011
REVISED MANUSCRIPT RECEIVED 16 OCTOBER 2011
MANUSCRIPT ACCEPTED 18 OCTOBER 2011

Printed in the USA